Consecutive Targetable Smart Nanoprobe for Molecular Recognition of Cytoplasmic microRNA in Metastatic Breast Cancer

Eunjung Kim,[†] Jaemoon Yang,[‡,¶,#] Joseph Park,[†] Soonhag Kim,[⊥] Nam Hee Kim,[§] Jong In Yook,[§] Jin-Suck Suh,[‡,#,▽] Seungjoo Haam,[†,#,*] and Yong-Min Huh[‡,#,▽,*]

[†]Department of Chemical and Biomolecular Engineering, [‡]Department of Radiology, and [§]Department of Oral Pathology, Oral Cancer Research Institute, College of Dentistry, Yonsei University, Seoul, Republic of Korea, [⊥]Department of Applied Bioscience, CHA University, Seoul 135-081, Republic of Korea, [¶]Severance Integrative Research Institute for Cerebral & Cardiovascular Diseases, Yonsei University Health System, Seoul 120-752, Republic of Korea, [#]YUHS-KRIBB Medical Convergence Research Institute, Seoul, 120-752, Republic of Korea, and [▽]Severance Biomedical Science Institute (SBSI), Seoul 120-749, Republic of Korea

ABSTRACT

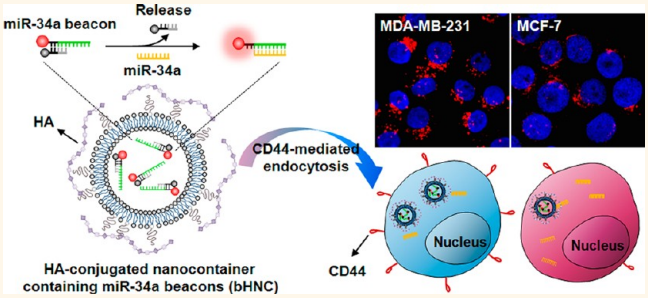

We report smart nanoprobe, hyaluronic acid (HA)-based nanocontainers containing miR-34a beacons (bHNCs), for the intracellular recognition of miR-34a levels in metastatic breast cancer cells, which is distinct from the imaging of biomarkers such of cell membrane receptors such as HER2. In this study, we demonstrate that a nanoscale vesicle that couples a targeting endocytic route, CD44, and a molecular imaging probe enables the efficient detection of specific miRNAs. Furthermore, bHNCs showed no cytotoxicity and high stability due to the anchored HA molecules on the surface of nanocontainers, and enables the targeted delivery of beacons *via* CD44 receptor-mediated endocytosis. *In vitro* and *in vivo* optical imaging using bHNCs also allow the measurement of miR-34a expression levels due to the selective recognition of the beacons released from the internalized bHNCs. We believe that the technique described herein can be further developed as a cancer diagnostic as well as a miRNA-based therapy of metastatic cancer.

KEYWORDS: miR-34a · molecular beacon · hyaluronic acid · nanocontainer · intracellular imaging

MicroRNAs (miRNAs) are small, noncoding RNA molecules that play a role as negative gene regulators and have been found to control various biological functions, such as cellular proliferation, differentiation, metastasis, and apoptosis.[1−3] Emerging evidence suggests that miRNAs can also function as a diagnostic biomarker and a therapeutic target for a wide range of diseases, including human cancers, because miRNAs themselves can act as tumor suppressor genes or oncogenes.[4−8] The primary challenge for developing miRNA-based therapeutics is effective strategy for the specific detection and delivery of miRNAs. The ability to image the intracellular distribution of specific miRNAs in an intact cell would provide insight into the causal mechanism of cancer metastasis and invasion.[9−11] Well-tailored nanostructures (*i.e.*, polymeric micelles, liposomes, polyplexes, *etc.*) have overcome many of these challenges due to the unique versatility of fabrication techniques and functionality, which protects miRNAs from degradation by endogenous nucleases and targets miRNAs to specific cells.[11−15] Among these nanostructures, nanocontainers (*i.e.*, liposomes) and their complex mixtures can carry more therapeutic and biologically useful molecules than other polymeric nanoplatforms, such as polymeric micelles and polyplexes.[16] In addition, PEGylated nanocontainers (PNCs) could overcome their poor stability by interactions with phospholipase and lipoproteins through the formation of a steric boundary.[17−19] We reasoned that our nanocarrier, in which a biocompatible polysaccharide was incorporated, could deliver a large amount of molecular beacons to target cells without the beacons leaking out. The systemic delivery using our nanocontainers is a major improvement over previously reported methods for delivering exogenous nucleic acid-based molecular beacons into cells, which used methods such as passive uptake, microinjection, cationic

* Address correspondence to haam@yonsei.ac.kr, ymhuh@yuhs.ac.

Received for review January 20, 2012 and accepted September 4, 2012.

Published online September 04, 2012
10.1021/nn300289u

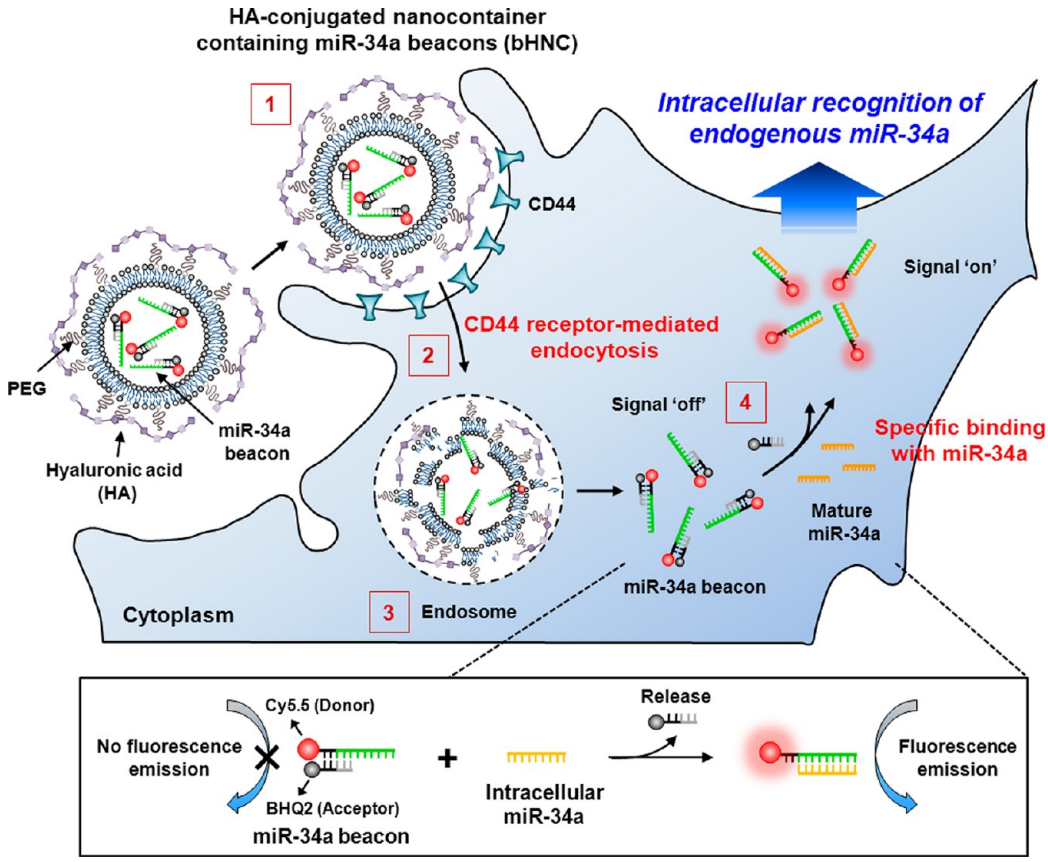

Figure 1. Schematic illustration of miR-34a beacon delivery system for targeted intracellular recognition of miR-34a based on HA-coated nanocontainers that encapsulate the miR-34a beacons (bHNCs); consecutive processes of (i) binding to CD44 receptors, (ii) internalization into an endosome, (iii) disassembling of bHNCs leading the destabilization of endosome membranes under pH reduction, and (iv) finally displacement of miR-34a beacons from the HNCs permitting transport into the cytoplasm.

transfection, and conjugation with cell penetrating peptides.[20−23]

In this report, we present the feasibility of stable and consecutive targetable nanoprobes for intracellular imaging of miR-34a expression levels in metastatic breast cancer as a model system (Figure 1). These nanocontainers involve (i) binding to CD44 receptors, (ii) internalization into an endosome, (iii) disassembling under pH reduction, leading the destabilization of endosome membranes, and (iv) finally displacement of miR-34a beacons from the nanocontainer permitting them to transport into the cytoplasm and bind intracellular miR-34a. In particular, hyaluronic acid (HA) as a nontoxic, nonimmunogenic, and biodegradable biopolymer with a wide range of molecular weight (10^3∼10^7 Da) has high affinity for the cell surface adhesion molecule cluster determinant 44 (CD44), which has been identified as the determinant of progression to the metastatic breast cancer because it rarely is seen in healthy tissue but is highly expressed in tumor cells with metastatic phenotype.[24−26] In addition to its principal mediator CD44, several cell-associated and extracellular HA binding receptors including the receptor for HA, receptor for endocytosis (HARE), HA-mediated motility (RHAMM or CD168), and intracellular adhesion molecule-1 (ICAM-1, or CD54) have been described for biological functions of HA.[27−29] Herein, we focused on CD44 as a main route for internalization of our nanoprobe and miR-34a as an imaging target, which is a tumor suppressor gene, and its upregulation induces cell-cycle arrest, senescence, apoptosis, and inhibition of migration.[30,31] The miR-34a expression which has also an important role in regulating CD44 could be a highly significant prognostic biomarker of metastatic cancer.[32] Thus, our sequential targeting system, which targets miRNA-specific molecular beacons *via* HA receptor-mediated endocytosis, enables intracellular imaging of miR-34a. Using HA-coated nanocontainers (HNCs) bearing miR-34a beacons (bHNCs), we achieved enhanced intracellular delivery, sustained release of miR-34a beacons, and targeted optical imaging of miR-34a in breast cancer cell lines. As proof-of-concept, we conducted *in vivo* optical imaging of an orthotopic breast cancer model for the evaluation of cytoplasmic miR-34a in tumor tissue.

RESULTS AND DISCUSSION

Design of a Molecular Beacon for Detection of Endogenous miR-34a. The optical imaging of miR-34a expression

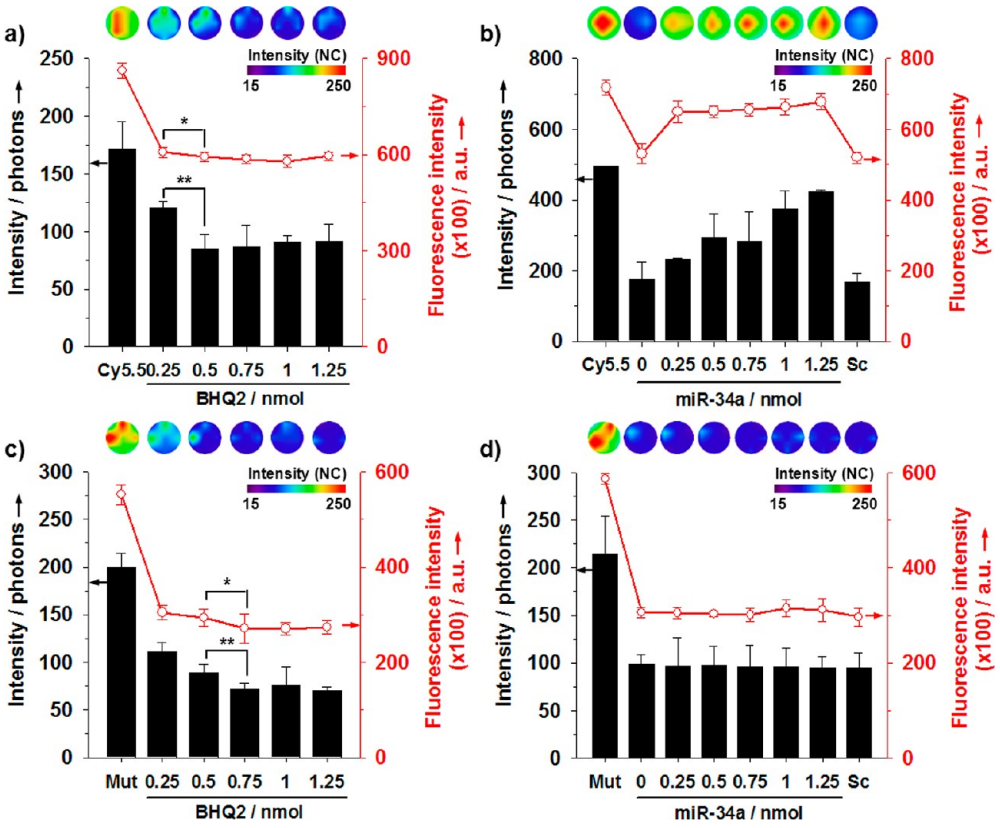

Figure 2. miR-34a beacons and specificity for the recognition of intracellular miR-34a. Fluorescence images (top of panels) and quantification of fluorescence intensity (bottom of panels) of microtubes containing different concentrations of (a) miR-34a beacons and (c) mutated beacons prepared by incubating a fixed concentration of Cy5.5-modified substrates (Cy5.5) or mutated Cy5.5-modified substrates (Mut) (0.25 nmol) with increasing concentrations of BHQ2-coupled oligonucleotides (BHQ2) (0.25, 0.5, 0.75, 1, and 1.25 nmol) at room temperature. Fluorescence images (top of panels) and quantification of fluorescence intensity (bottom of panels) of mixtures of each beacon (b) miR-34a beacons or (d) mutated beacons) and various concentrations of synthetic miR-34a oligonucleotides (0, 0.25, 0.5, 0.75, 1, and 1.25 nmol). Scrambled miR-34a oligonucleotides (Sc) were used as a negative control: $*p$ and $**p < 0.01$. The intensity maps on the fluorescence images are displayed in the normalized photon counts (NC) with laser power (0.8 μW) and integration time (1.0 s) per points.

level of breast cancer cells was based on the fluorescence resonance energy transfer (FRET) system. Linear oligonucleotides that are complementary to miR-34a were conjugated to an organic fluorophore (Cy5.5) as a fluorescent donor and annealed to a shorter oligonucleotide that was conjugated to a black hole quencher2 (BHQ2) as a fluorescent acceptor. These annealed complexes were synthesized as miR-34a beacons. The quenching efficiency of miR-34a beacons was determined by annealing a fixed concentration of Cy5.5-modified oligonucleotides (0.25 nmol) with increasing concentrations of quencher conjugated oligonucleotides. The fluorescence intensity of the prepared miR-34a beacons was gradually quenched with increasing amounts of the quencher coupled oligomers (Figure 2a). The fluorescence analysis of miR-34a beacons and their quantitative analysis were also validated using an optical imaging instrument and a fluorometer, resulting in the maximal quenching efficiency (56.6 $\pm$ 2.7%) given by 100 $\times$ (1 $-$ photon $\text{counts}_{\text{with quencher}}$/photon $\text{counts}_{\text{without quencher}}$) at 0.75 nmol of the Cy5.5-modified oligonucleotides (Figure 2a). Consequently, to maximize their quenching efficiency for the synthesis of molecular beacons, we set the optimal BHQ2/Cy5.5 molar ratio at 3. In the presence of the beacon's target, the 22-nucleotide mature miR-34a, the fluorescence signal of the miR-34a beacons is restored with increasing amounts of miR-34a. Hybridization with 1.5 nmol miR-34a increased the fluorescence intensity of the beacons to 94.5% of the unquenched Cy5.5-modified oligonucleotide solution. This was due to the "displacement hybridization" process which causes a significant effect on molecular beacon's thermodynamic equilibrium state induced by the changes in the length of binding region.[33−36] Consequently, hybridization between the miR-34a beacon and miR-34a occurs simultaneously to form more stable structures than the previously formed duplexed ones because of the longer binding site of a target than a quencher-labled oligonucleotide. In contrast, the miR-34a beacons treated with scrambled target oligonucleotides remained quenched (Figure 2b). We also synthesized mutated miR-34a beacons with 5-base-mismatched sequences (mutated beacons) as a negative control which resulted in similar quenching efficiency (55.8 $\pm$ 2.5%) to that of miR-34a beacons at the

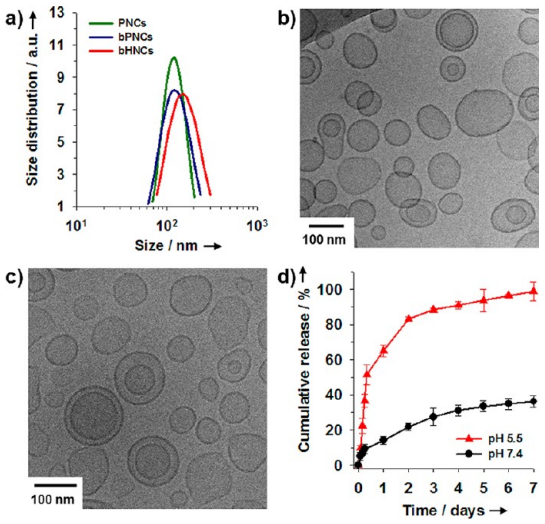

Figure 3. Formulation and characterization of bHNCs. (a) Size distribution of PNCs, bPNCs, and bHNCs, respectively. Cryo-TEM images of (b) PNCs and (c) bPNCs. (d) Release profile of miR-34a beacons from bHNCs at 37 °C in phosphate-buffered saline (pH 5.5 and pH 7.4) for 7 days (n = 3, error bars represent a standard deviation).

BHQ2/Cy5.5 molar ratio of 3, while the fluorescence signals of the mutated beacons remained quenched after incubation with miR-34a oligonucleotides (Figure 2c,d). These results suggest that miR-34a beacons can specifically bind the target oligonucleotide (miR-34a) for the noninvasive imaging of endogenous miRNA expression levels *in vitro* and *in vivo*.

HA-Conjugated Nanocontainers for HA Receptor-Guided Delivery of miR-34a Beacons. To maximize the delivery amount of miR-34a beacons, we first formulated PNCs according to a previously described hydration/extrusion method.[37] The miR-34a beacon-containing PNCs (bPNCs) were then prepared by direct lipid film hydration with a miR-34a beacon solution. The bPNCs showed a slight increase in size (129.4 ± 0.5 nm; polydispersity index, PDI, 0.13) and a reduced surface charge (−6.8 ± 3.3 mV) than PNCs without beacons (size, 124.0 ± 2.7 nm; PDI, 0.11; zeta potential, 2.2 ± 1.6 mV), which was likely due to incorporation of negatively charged miR-34a beacons (Figure 3a). The observed PNC and bPNCs morphology by cryo-transmission electron microscopy (cryo-TEM) showed spherical unilamellar vesicle structures without any aggregation regardless of miR-34a beacon loading (Figure 3b,c). These results confirmed that PNCs have beacon-loadable potentials for optical imaging of endogenous miRNA expression level.

For targeted delivery of miR-34a beacons to CD44-overexpressing cancer cells, on the other hand, HA-conjugated bPNCs (bHNCs) were prepared by conjugating activated HA (10^6 Da) and bPNCs at a molar ratio of 0.01, resulting in an increase in mean size (151.6 ± 9.4 nm; PDI, 0.14) and a decrease in zeta potential (−12.8 ± 4.5 mV) (Figure 3a and Supporting Information Figure S1). This was due to the addition of high molecular weight and negatively charged HA molecules onto the bPNC surface. The increased negative charge and additional steric hindrance[38] due to anchoring HA onto bPNCs may provide long-term stability of these particles in an aqueous condition.[39,40]

To confirm the release profile under the biological environment, we examined the miR-34a beacon release behavior under various pH values (pH 5.5 and 7.4) at 37 °C (Figure 3d, Supporting Information Figures S2 and S3). Notably, the miR-34a beacons at acidic condition were released more quickly than at neutral conditions and approximately 65% and 14% of beacons, respectively, were released within 24 h. After 7 days, more than 95% of miR-34a beacons were released from bHNCs because of the destabilization of liposomal structures[41] and the biodegradation of HA under low pH. In particular, the degradation of HA in aqueous solution is caused by hydrolysis attributed to the random scission of its polymer chains, and its degradation rate strongly depends on pH, exhibiting that HA is more labile in acidic condition than neutral condition.[42,43] Thus, while bHNCs showed a slow release profile due to HA attachment to the surface of bPNCs at neutral pH, the release rate is suddenly accelerated at low pH, implying that bHNCs is a suitable nanoplatform for the selective imaging of the endogenous miR-34a expression level.

***In Vitro* Intracellular Imaging of miR-34a Using bHNCs.** To measure endogenous miR-34a expression level in breast cancer cells, we first selected MCF-7 cells, containing wild-type p53, and MDA-MB-231 cells, containing mutant p53, because previous research has shown that miR-34a, one of the miR-34 family members, is a direct transcriptional target of p53.[6,30,31] Additionally, its functional activity indicates a potential role as a metastatic tumor suppressor.[30,31] Using a quantitative reverse transcription polymerase chain reaction (qRT-PCR), we found that miR-34a expression levels were significantly higher in MCF-7 cells than in MDA-MB-231 cells, which is consistent with previous reports showing that *in vitro* and *in vivo* miR-34a levels are increased in a p53-dependent manner (Figure S4a in Supporting Information).[30,31] Next, we examined the percentage of CD44-positive cells in MCF-7 and MDA-MB-231 cells using flow cytometry. Metastatic MDA-MB-231 cells (98.8%) expressed much higher levels of CD44 than less invasive MCF-7 cells (3.6%), as shown in Figure S4a in Supporting Information. The expression level of miR-34a in each breast cancer cell line did not correspond with that of CD44 receptor expression because miR-34a is a negative regulator of the CD44 receptor,[32] suggesting strong correlations between these two factors, which further validates the prepared bHNCs as a feasible option for monitoring intracellular miR-34a levels in these human breast cancer cells (Figure S4b in Supporting Information).

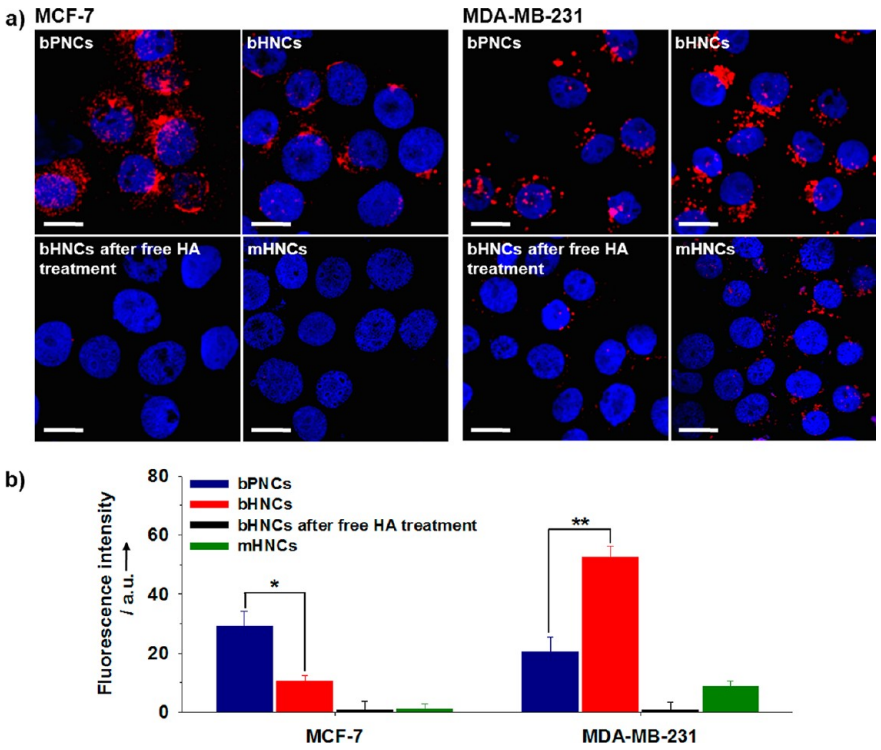

Figure 4. *In vitro* **imaging of intracellular miR-34a in breast cancer cells. (a) Confocal microscopic images and (b) fluorescence intensity of MCF-7 and MDA-MB-231 cells incubated for 4 h with bPNCs, bHNCs, bHNCs after preincubation for 2 h with free HA (5 mg/mL), and mHNCs, respectively (miR-34a beacon concentration, 1 nmol): blue, Hoechst 33342 (nucleus staining); red, Cy5.5 (miR-34a beacons). The total intensity of Cy5.5 fluorescence was measured in the counted cells (5×10^4 cells) of each condition. All scale bars are 20 μm. ($n = 3$, error bars represent a standard deviation, *p and **$p < 0.001$).**

To assess the cytotoxicity of bHNCs, we evaluated the viability of target cancer cells (MCF-7 and MDA-MB-231) treated with bHNCs at concentrations ranging from 2 to 32 μM and with incubation times of 24 or 48 h using an MTT assay. As in Figure S5 (Supporting Information), no significant proliferation inhibition was exhibited with up to 32 μM and for a 48 h incubation, revealing that bHNCs have high biocompatibility.

To validate the utility of bHNCs as an intracellular imaging agent, we targeted both CD44 and miR-34a with bPNCs or bHNCs. Fluorescence images of MCF-7 and MDA-MB-231 cells treated with bPNCs or bHNCs (miR-34a beacons: 1 nmol) were obtained using confocal microscopy (Figure 4a). After treatment of MCF-7 cells with bPNCs, a significantly greater increase in Cy5.5 fluorescence was observed than treatment of MDA-MB-231 cells. This result is consistent with the levels of mature miR-34a previously determined using qRT-PCR analysis.

Next, we determined whether bHNCs-delivery of miR-34a beacons could be utilized to assess the cytoplasmic distribution of miR-34a. MDA-MB-231 and MCF-7 cells were treated with bHNCs, and a greater number of red spots were observed in the cytoplasm of MDA-MB-231 cells than MCF-7 cells. This was likely due to a higher CD44 expression level on MDA-MB-231 cells, though MCF-7 cells have higher miR-34a expression levels. To verify whether bHNCs are internalized *via* a specific interaction with the CD44 receptor, the ligand blocking assay, using 5 mg/mL free HA, was performed, as described previously.[44] Pretreatment of cells with HA suppressed bHNCs uptake, indicating that free HA blocked the CD44 receptor. Since MCF-7 and MDA-MB-231 cells express different CD44 levels, the CD44 target-specificity of bHNCs correlated with the beacon signal after bHNCs-treatment. The fluorescence intensity was 5-fold higher after uptake of bHNCs into MDA-MB-231 cells than into MCF-7 cells. However, bHNCs uptake was completely suppressed after excess free HA treatment due to blocking of the CD44 receptors (Figure 4a,b). The ligand blocking assay against bPNCs was further performed to enhance the targeting effects of HA so that only bHNCs were internalized by CD44 receptor-mediated endocytosis (Figure S6 in Supporting Information). It was observed that both cancer cell lines incubated with bPNCs after the postincubation with free HA exhibited similar fluorescence intensity compared with that in only bPNCs treated-cells, revealing that the mechanism for intracellular delivery of bPNCs was a CD44 receptor-independent endocytosis. Subsequently, the mutated beacons-containing HNCs (mHNCs) as a negative control were formulated for the miR-34a target-selectivity. As expected, both cells treated with mHNCs showed significantly reduced fluorescence intensity compared to those treated with bHNCs, even though

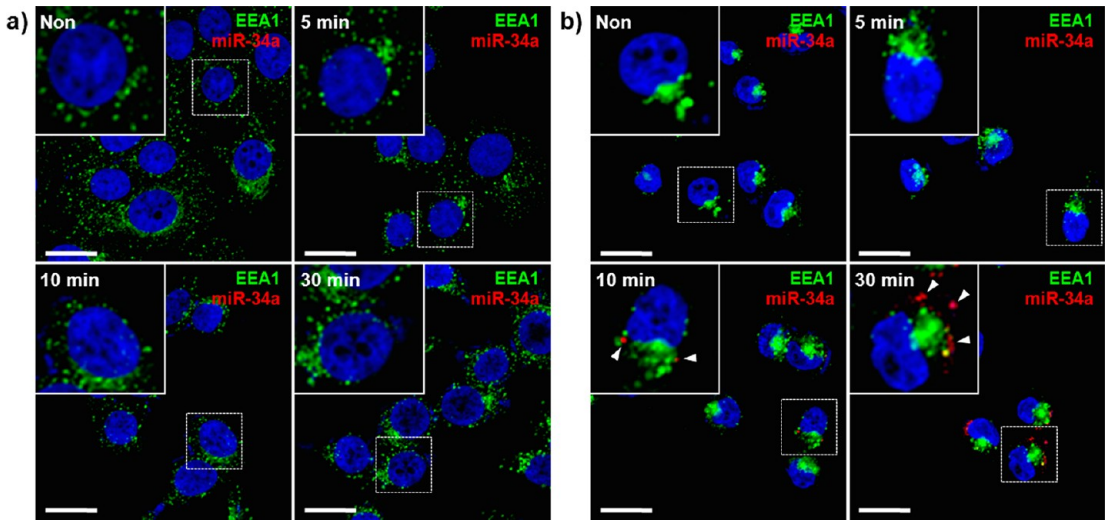

Figure 5. Endocytic trafficking of bHNCs in breast cancer cells. Confocal images of (a) MCF-7 and (b) MDA-MB-231 cells treated with bHNCs for 10 min at 37 °C, replenished with free culture media, and incubated for the indicated time intervals (5, 10, and 30 min): blue, Hoechst 33342 (nucleus staining); green, Alexa Fluor 488 (EEA1 staining); red, Cy5.5 (miR-34a beacons). All scale bars are 20 μm.

some fluorescence intensity in MDA-MB-231 cells treated with mHNCs was generated by background signals of quenched beacons (Figure 4a,b). These results demonstrated that bHNCs not only enhanced cellular uptake by CD44 receptor-mediated endocytosis but also selectively detected miR-34a in breast cancer cells.

Several studies have demonstrated that EGFR and ErbB2 are functionally linked with CD44 in cancer cells and influence intramembrane processing of CD44 such as CD44 internalization and cleavage.[45−47] Therefore, we tested whether bHNCs are internalized into both EGFR-negative MCF-7 cells and EGFR-positive MDA-MB-231 cells when the cells were pretreated with lapatinib, a commercially available tyrosine kinase inhibitor interrupting the function of EGFR and ErbB (Figure S7 in Supporting Information). Since lapatinib prevents EGFR and ErbB2 from being activated, a significant reduction of signals from bHNCs was observed in MDA-MB-231 in a dose-dependent manner of lapatinib. In particular, the fluorescence intensity was decreased 96% when cells were treated with 0.5 μM of lapatinib, whereas the lapatinib treatments did not have any effect on bHNCs uptake to MCF-7 cells that highly expressed ICAM-1 (CD54).[48] These results support that bHNCs uptake depends not only on HA receptors but also on the EGFR/ErbB activity in cancer cells.

We also assessed the *in vitro* targeting ability of bHNCs in MCF-10 cells, nontumorigenic breast epithelial cell lines. Likewise, although a high level of miR-34a was detected in MCF-10A cells, a decrease in fluorescence signals due to low CD44 expression was displayed when the cells were treated with bHNCs. Of course, the performance of bHNCs was also tested in the A549 lung cancer cell line, and similar results were obtained because A549 cells have high expression levels of both miR-34a and the CD44 receptor (Figure S4 and S8 in Supporting Information). These results demonstrate that bHNCs were selectively internalized by the CD44 receptor-mediated endocytosis. Also, they sustainably released molecular beacons from HA-modified carriers, and theses beacons successfully bound endogenous miR-34a with high enough specificity to produce a fluorescent signal. Thus, using bHNCs is a feasible approach to measure the expression levels of miR-34a in a variety of human cancer cells.

Subcellular Localization of bHNCs. To demonstrate the endosomal escape of the released miR-34a beacons from internalized bHNCs, we further performed colocalization experiments in both MCF-7 and MDA-MB-231 cells with an early endosome marker (early endosomal antigen 1, EEA1) and a late endosome/lysosome marker (lysosome associated membrane protein 1, LAMP1). Confocal microscopic images of MCF-7 and MDA-MB-231 cells reveal that endogenous miR-34a in MDA-MB-231 cells has a distributed punctate pattern without colocalization with endosomes or lysosomes in a cytoplasm after 10 min, and the increased miR-34a expression was found at 60 min (Figures 5 and 6, and Supporting Information Figures S9 and S10). In particular, the examination of images of a single cell at high magnifications showed the heterogeneous distribution of miR-34a beacons with red fluorescence, which suggests that they might be still confined in the nanocontainers or other subcellular compartments after endosomal escape (Figures 5b and 6b). Because the detection of miR-34a using our molecular beacon represents a signal-on system, bHNCs were "off-state" after internalization into an early endosome, resulting in no Cy5.5 fluorescence for 1 and 5 min incubation, respectively. In contrast, no Cy5.5 fluorescence was observed in MCF-7 cells due to low uptake efficiency of bHNCs. From these results, we conclude that bHNCs

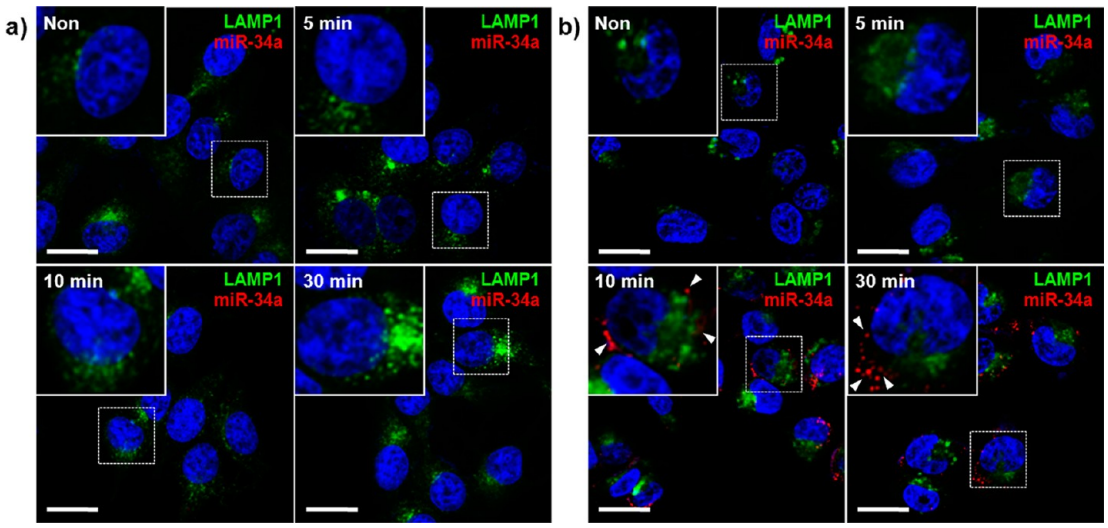

Figure 6. Endocytic trafficking of bHNCs in breast cancer cells. Confocal images of (a) MCF-7 and (b) MDA-MB-231 cells treated with bHNCs for 10 min at 37 °C, replenished with free culture media, and incubated for the indicated time intervals (5, 10, and 30 min): blue, Hoechst 33342 (nucleus staining); green, Alexa Fluor 488 (LAMP1 staining); red, Cy5.5 (miR-34a beacons). All scale bars are 20 μm.

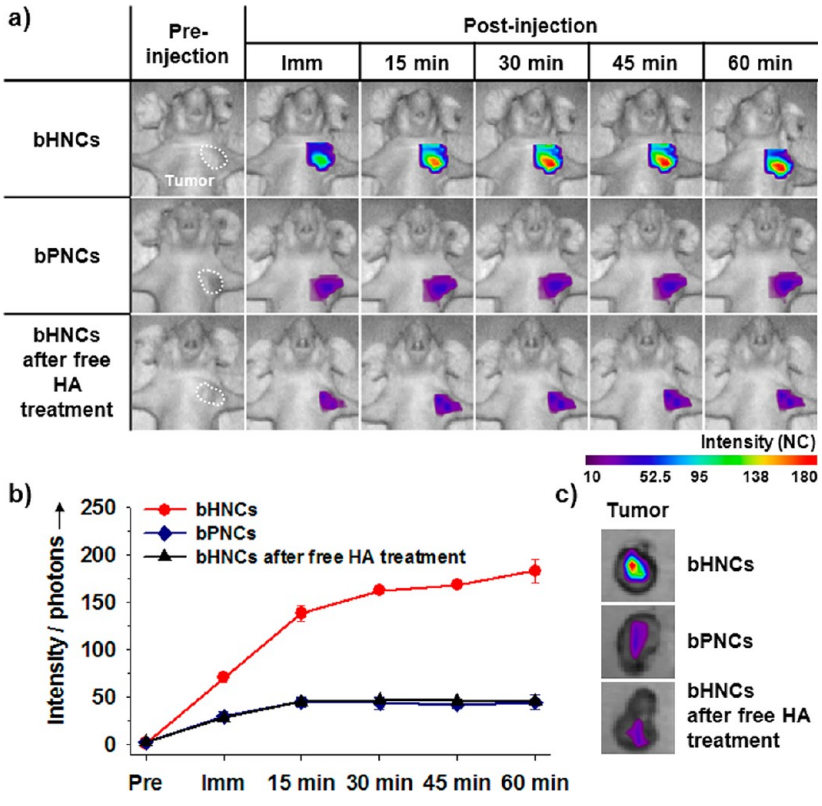

Figure 7. *In vivo* and *ex vivo* imaging of miR-34a in an orthotopic breast cancer model. (a) *In vivo* optical fluorescence images of MDA-MB-231 tumor-bearing mice after the intravenous injection of bHNCs, bPNCs, and bHNCs after free HA treatment (10 mg/mL of HA in PBS per animal) at various time intervals, respectively. Tumor regions are indicated with a white dashed boundary. (b) Total photon counts in tumor region after injection of bHNCs, bPNCs, and bHNCs after free HA treatment (miR-34a beacon concentration, 5 nmol). (c) *Ex vivo* optical fluorescence images of tumors excised at 1 h postinjection of bHNCs, bPNCs, and bHNCs after free HA treatment, respectively. The intensity maps on the fluorescence images are displayed in the normalized photon counts (NC) with laser power (5.0 μW) and integration time (0.4 s) per points.

were internalized *via* HA receptor-dependent endocytosis and efficiently underwent cytoplasmic diffusion without confinement or degradation inside endosome and lysosome vesicles.

***In Vivo* Optical Imaging Using bHNCs.** Finally, we performed *in vivo* optical imaging using bHNCs to examine whether the intravenously injected bHNCs could selectively detect miR-34a in a breast cancer cells.

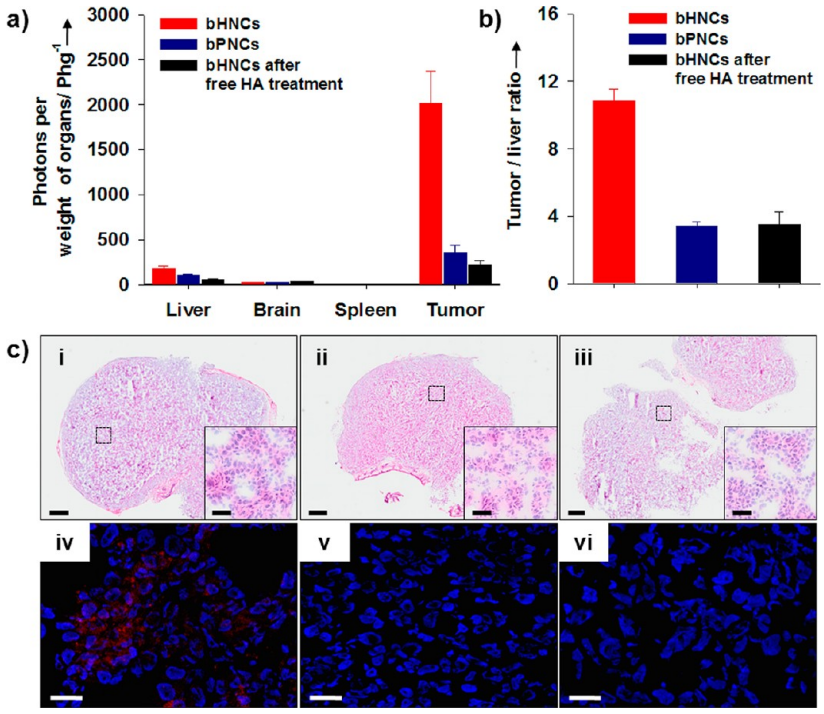

Figure 8. Biodistribution and tumor tissue localization of bHNCs after intravenous injection. (a) Quantification of *ex vivo* biodistribution of bHNCs and bPNCs recorded as total photon counts per each excised organ and tumor weight at 1 h postinjection. (b) The ratios of the photon counts of tumor to that of liver. ($n = 3$, error bars represent a standard deviation) (c) The entire H&E staining (i−iii) and confocal microscopy images (iv−vi) of tumor injected with bHNCs (i and iv), bPNCs (ii and v), and bHNCs after free HA treatment (iii and vi), respectively (upper scale bar, 500 μm; lower scal bar, 20 μm). The inset images indicate the dashed square section of the entire image at high magnification (scale bar, 40 μm). The tumor section was counterstained with Hoechst 33342 (blue) for nucleus. The red color means Cy5.5 from miR-34a beacons.

To develop a CD44-positive orthotopic breast tumor model, MDA-MB-231 cells were transplanted into the mammary fat pad of nude mice. Using our nanoprobe, *in vivo* miR-34a expression levels could be directly monitored with noninvasive and real-time fluorescence imaging (Figure S11 in Supporting Information). Figure 7 shows typical time-dependent images of mice and the emitted photons from tumor region for 1 h after the intravenous injection of bHNCs, bPNCs, and bHNCs (miR-34a beacons, 5 nmol) following pretreatment with 10 mg/mL free HA, respectively. At this time point, bHNCs injection provided a strong fluorescence signal in CD44-positive tumor bearing mice, while both bPNCs and blocking groups using excess HA as controls showed a significantly reduced fluorescence signals compared to bHNCs, which were consistent with previous *in vitro* studies. Considering these results, our nanoplatforms were effective for characterization of tumor expressing miR-34a due to their binding ability to CD44 and targetable recognition of miR-34a.

We also confirmed the tumor-specific delivery of bHNCs by *ex vivo* fluorescence signals of immediately excised tissues (liver, brain, spleen, and tumor) after *in vivo* imaging experiments (Figure 8). The total fluorescence signals of tumor excised from the mice treated with bHNCs was stronger than that treated with bPNCs and bHNCs after post-treatment of free HA, respectively, which is agreement with the *in vivo* imaging results (Figure 8a). Because HA receptors, RHAMM and ICAM-I, are also rich in endothelial cells of liver, lymph node, and spleen,[49] a certain amount of bHNCs might be accumulated in other organs. However, the predominant accumulation of bHNCs was obviously observed in the tumor region than in other organs. The ratios of the photon counts of tumor to that of liver were depicted in Figure 8b (bHNCs, 10.8 ± 0.7; bPNCs, 3.4 ± 0.3; and bHNCs after free HA treatment, 3.5 ± 0.7).

The excised tumor was positive for proliferating tumor cells, according to the histological analysis of tumor tissue sections using Hematoxylin and Eosin stains. Confocal microscopy images of frozen tumor sections revealed that Cy5.5 fluorescence intensity was clearly seen in the only group treated with bHNCs (Figure 7c). Our results collectively confirm the feasibility of utilizing bHNCs for detection and visualization of specific miR-34a expression in breast cancer animal models.

CONCLUSION

We have formulated HA-coated nanocontainers for the efficient intracellular delivery of miR-34a beacons, allowing targeted optical imaging of specific miRNA species. These smart nanoprobes are designed to be endocytosed by CD44-overexpressing cancer cells, and then to deliver miR-34a-specific molecular beacons,

so-called a sequential targeting system. They could also be used to deliver miRNAs into human cancer cells for a certain gene set knockdown therapy. These nanoparticles represent a promising new platform for diagnostic imaging and RNA-based cancer therapy due to their low toxicity and ability to be targeted. Therefore, the monitoring of miRNAs in human cancer and their delivery using our HNCs encapsulating molecular beacons and/or therapeutic miRNAs would facilitate simultaneous cancer therapy and diagnosis.

METHODS

Preparation and Characterization of Molecular Beacons. Molecular beacons for imaging of miR-34a were synthesized with a Cy5.5 donor conjugated to its 5′-terminus and a black hole quencher 2 (BHQ2)-coupled oligomers to its 3′-terminus as an acceptor, which were obtained from Bioneer Inc. (Daejeon, Korea). The entire sequences of miR-34a beacons were as follows: 5′-Cy5.5-TTC GCT GTA CAA CCA GCT AAG ACA CTG CCA-3′, 3′-BHQ2-GCG ACA TGT TG-5′. For the site-specificity of miR-34a beacons, we mutated the five regions in the Cy5.5-labeled oligonucleotides as a negative control: 5′-Cy5.5-TTC GCT GTA CAA CC***G*** GC***C*** AAG AC***G*** ***T***TG CC***G***-3′. Both oligomers were mixed at different molar ratios and annealed at 95 °C for 4 min and then at 70 °C for 10 min, followed by slow cooling to room temperature. For the analysis of efficient fluorescence quenching, the fluorescence intensity of the each prepared miR-34a beacons and mutated beacons (100 μL) was measured by a hybrid multimode microplate reader (Synergy H4, BioTek, USA) at 670 nm excitation and 690 nm emission. Near-infrared (NIR) fluorescence images were obtained with an eXplore Optix system (ART, Advanced Research Technologies, Montreal, Canada). Laser power and integration time were optimized at 0.8 μW and 1.0 s per point, respectively. Excitation and emission spots were raster-scanned in 1 mm steps over the selected region of interest to generate emission wavelength scans. A 670 nm pulsed laser diode was used to excite Cy5.5 molecules, and NIR fluorescence emission at 690 nm was collected with a fast photomultiplier tube (Hamamatsu, Japan). Images were presented by the image maps of fluorescence intensity using Analysis Workstation software (ART) and the fluorescence intensity was expressed as the normalized photon counts with laser power and integration time, calculated by the following equation: normalized counts (NC) = total photon counts/[laser intensity (μW) $\times$ integration time (sec)].

Formulation of Beacon-Containing Nanocontainers. Three lipids, L-α-phosphatidylcholine (PC), β-cholestanol (Chol), and 1,2-distearoyl-*sn*-glycero-3-phosphoethanolamine-*N*-[amino(polyethylene glycol)-2000] (DSPE-PEG2000 Amine), were purchased from Avanti Polar Lipids Inc. (Alabaster, AL, USA). Lipid mixtures of PC, Chol, and DSPE-PEG2000 Amine with a molar ratio of 2:1:0.15 were dissolved in chloroform. The chloroform was then removed by rotary vacuum evaporation to form a thin lipid film on the round-bottom flask, which was placed for additional 1 h under high vacuum to remove any residual chloroform. The dried lipid film was directly hydrated overnight at 4 °C using a solution containing 1 nmol of prepared miR-34a beacons in HBS buffer (100 mM NaCl, 20 mM HEPES/NaOH buffer, pH 7.5, 0.02% w/v sodium azide) and then magnetically stirred for 1 h at room temperature, resulting in bPNCs. The bPNCs solution was finally extruded 10 times using a mini-extruder (Avanti Polar Lipids), through a polycarbonate membrane filter with 100 nm pores. Afterward, bPNCs were purified using a Sephadex column (SephadexTM G-75, GE Healthcare, UK) to remove free miR-34a beacons. The mPNCs were prepared in the same manner as bPNCs. The obtained bPNCs and mPNC were stored at 4 °C until use.

To prepare bHNCs and mHNCs, the *N*-hydroxysuccinimide ester groups of HA were respectively reacted for 4 h at room temperature with amine groups on the surface of bPNCs and mPNCs due to the use of DSPE-PEG2000 amine, creating a stable amide bond. The average hydrodynamic diameters and zeta potentials of the prepared bHNCs were measured by laser scattering (ELS-Z, Otsuka Electronics, Japan).

Cryotransmission Electron Microscopy. For cryotransmission electron microscopy (cryo-TEM), 4 μL of PNCs and bPNCs (1 mM) were respectively suspended onto 300 mesh holey carbon grids (Agar scientific, U.K.) that had not been pretreated. Theses grids were then blotted using an FEI Vitrobot, Mark I (FEI, USA), with the setting of 100% humidity, 4 °C, and blot time of 2.5 s. The vitreous ice sample grids were maintained at a temperature of around −178 °C within the electron microscope using a side-entry Gatan 626 cryo-holder (Gatan, USA). These grids were examined in a Technai G2 Spirit Twin transmission electron microscope fitted with anticontaminator (FEI, USA) operated at 120 kV. Images were recorded on a 4K $\times$ 4K, Ultrascan 895 CCD camera (Gatan, USA). For cryo-TEM, a low-dose method (exposures at 1000 electrons per nm^2/s) was used, and underfocus values used for imaging on the sample area were 2.7 μm.

Release Study of miR-34a Beacons. bPNCs and bHNCs were suspended in 2 mL of PBS (10 mM, pH 5.5 and 7.4) (30 μM), sealed in a dialysis tube with a molecular weight cut off of 50 000 Da (Tube-O-Dialyzer, G-Biosciences, St Louis, MO, USA), and then immersed in 10 mL of buffer solution at 37 °C. The system was moderately shaken, and the amount of released miR-34a beacons was monitored at an absorbance of 260 nm using a biophotometer (BioPhotometer plus, Eppendorf, Hamburg, Germany). The concentration of encapsulated miR-34a beacons in the HNCs (286.9 μg/mg lipid) was measured in the same manner with or without Triton-X for solubilization of liposomes, and its encapsulation efficiency (60.9%) was calculated by the following equation: (amount of beacons in nanocontainers)/(total amount of beacons) $\times$100.

Cell Culture and Intracellular Imaging of miR-34a. Human breast cancer cell lines MCF-7 and MDA-MB-231, human lung cancer cell line A549, and nontumorigenic human breast epithelial cell line MCF-10A were obtained from American Tissue Type Culture (ATCC, Rockville, MD, USA). MCF-7 and A549 cells were cultured in DMEM medium (Gibco, Invitrogen, Grand Island, NY, USA) supplemented with 10% fetal bovine serum (FBS) and 1% antibiotics. MDA-MB-231 cells were cultured in RPMI 1640 medium (Gibco, Invitrogen) containing 5% FBS and 1% antibiotics. MCF-10A cells were cultured in DMEM/F12 medium (Gibco, Invitrogen) supplemented with 5% horse serum, 20 ng/mL epidermal growth factor, 0.5 mg/mL hydrocortisone, 100 ng/mL cholera toxin, 10 μg/mL insulin, and 1% antibiotics. All cultures were maintained at 37 °C in a 5% CO_2 atmosphere. MCF-7, MDA-MB-231, A549, and MCF-10A cells (10^6 cells/well) were plated into 6-well plates and incubated overnight. The medium was replaced with 500 μL of serum-free medium, and 500 μL of bHNCs and mHNCs (2 μM) were added to each well, followed by incubation for 4 h at 37 °C. For inhibition tests, excess HA (5 μM) was pretreated and incubated for 2 h at 37 °C prior to treatment. To test EGFR/ErbB dependence on bHNCs uptake, different concentrations of lapatinib purchased from Selleck Chemicals was pretreated and incubated for 2 h at 37 °C. The treated cells were trypsinized and washed twice with PBS (10 mM, pH7.4). For nucleus staining, the collected cells were incubated with Hoechst 33342 (Invitrogen, 1 μg/mL) for 5 min at room temperature, rinsed twice with PBS (10 mM, pH7.4), and then transferred to a glass slide by cyto-spin (8000 rpm, 4 min). After drying of the glass slide, the intracellular localization of miR-34a was observed using a laser scanning confocal microscope (LSM700, Carl Zeiss, Jena, Germany) with a 63$\times$ water immersion objective at 670 nm excitation and 690 nm emission wavelengths. For the quantitative analysis, the fluorescence intensity of the gathered cells was determined by a hybrid multimode microplate reader (Synergy H4, BioTek) at 670 nm excitation and 690 nm emission.

Immunocytochemistry Stains. It is well documented that the delivery mechanisms of liposome-mediated oligonucleotides

involve (i) direct fusion of liposomes with endosome membranes and/or (ii) destabilization of endosomes by disruption of liposomal structures.[50−52] On the basis of the proposed mechanisms, our nanocontainers mainly composed of dioleoylphosphatidylcholines and dioleylphosphatidylethanolamine are expected to induce the destabilization of the liposome and endosomal membranes because the protonation of their amine head groups by acidification facilitates changes in their geometrical shape. To track the internalization of bHNCs, MDA-MB-231, MCF-7, and A549 cells were grown on glass coverslips (5×10^4 cells/well of 24-well plates) and incubated overnight. Subsequently, the cells were rinsed twice with PBS and treated with bHNCs (2 μM) in 500 μL serum free media. After 10 min incubation with bHNCs at 37 °C, the culture media was changed with fresh ones. At predetermined time intervals, the cells were washed twice with PBS and then, fixed in 4% paraformaldehyde in PBS for 10 min. The fixed cells were permeabilized with 0.1% Triton X-100 in PBS for 10 min, blocked with 1% bovine serum albumin (BSA) in PBS for 1 h, and stained with rabbit polyclonal anti-EEA1 (abcam # ab2900, Cambridge, MA, USA) or mouse monoclonal anti-LAMP1 (abcam # ab25630) diluted in PBS containing 1% BSA (1:200) for 1 h. After being washed three times with PBS to remove excess antibodies, the cells were incubated with the secondary antibody of goat antirabbit IgG conjugated with Alexa Fluor488 (Invitrogen) or antimouse IgG conjugated with fluorescein diluted in PBS containing 1% BSA (1:300) for 1 h. The stained cells were counterstained to visualize the nucleus by Hoechst 33342 (Invitrogen, 1 μg/mL) and examined using a laser scanning confocal microscope (LSM700, Carl Zeiss, Jena, Germany). All cell staining procedures were performed at room temperature.

Optical Imaging of Orthotopic Breast Cancer Model. All animal experiments were conducted with the approval of the Association for Assessment and Accreditation of Laboratory Animal Care (AAALAC) International. *In vivo* optical fluorescence imaging to detect miR-34a in breast cancer, we developed orthotopic breast cancer model by injection of MDA-MB-231 cells[7,26,53] (10^7 cells suspended in 200 μL of PBS per animal) into the left mammary fat pad of female BALB/c-nude mice, 4−5 weeks of age, under anesthesia (a 3:1 mixture of Zoletil/Rompun). Near-infrared (NIR) fluorescence tomographic images were obtained with an eXplore Optix system (ART, Advanced Research Technologies, Montreal, Canada). Imaging was performed for 1 h after injection of naked miR-34a beacons, bHNCs, bPNCs, and bHNCs (miR-34a beacons, 5 nmol) with postinjection of free HA (10 μM) and the obtained images were assessed with an Analysis Workstation (ART, Advanced Research Technologies). After intravenous injection of each solution of 200 μL bHNCs and bPNCs into mouse tail veins (25 μM), the fluorescence profiles in MDA-MB-231 tumor-bearing mice were imaged by positioning mice on an animal plate heated to 37 °C in the eXplore Optix system. The animal was automatically moved to the imaging chamber for scanning. Laser power and integration time were optimized at 5.0 μW and 0.4 s per point, respectively. Excitation and emission spots were raster-scanned in 1 mm steps over the selected region of interest to generate emission wavelength scans. A 670 nm pulsed laser diode was used to excite Cy5.5 molecules and NIR fluorescence emission at 690 nm was collected with a fast photomultiplier tube (Hamamatsu, Japan). After 1 h, the mice were sacrificed and the selected organs (liver, spleen, brain, and tumor) in mice of each group (bHNCs, bPNCs, and bHNCs after free HA treatments) were excised, then kept in saline. The relative photon counts in the excised organs were calculated by dividing total photon counts in organs by the weight of individual organs, respectively.

Statistical Analysis. The statistical evaluation of data was performed using an analysis of variance (Student's *t* test). A *p*-value of less than 0.001 was considered statistically significant.

Conflict of Interest: The authors declare no competing financial interest.

Acknowledgment. This work was supported by National Research Foundation of Korea Grant funded by the Korean Government (MEST) (2010-0019923) and a grant of the Korea Health 21 R&D Project, Ministry of Health & Welfare, Republic of Korea (A085136). We are grateful to Korea Basic Science Institute (Daejeon) for the valuable support in the cryo-TEM measurements and Yonsei-Carl Zeiss Advanced Imaging Center, Yonsei University College of Medicine, for technical assistance.

Supporting Information Available: Methods: activation of HA, evaluation of miR-34a and CD44 expression levels in each cell, and *in vitro* cell viability test. Results on ^{1}H NMR spectrum of activated HA, release kinetics of miR-34a beacons, the expression levels of miR-34a and CD44 *via* qRT-PCR and flow cytometric analysis, and cytotoxicity of bHNCs; data about ligand blocking assay against bPNCs, EGFR/ErbB-dependent intracellular uptake of bHNCs, the performance of bHNCs in nontumorigenic breast MCF-10A cells and lung cancer A549 cells, endosomal escape of bHNCs, *in vivo* optical imaging at different time intervals, and *in vivo* optical imaging using naked miR-34a beacons. This material is available free of charge via the Internet at http://pubs.acs.org.

REFERENCES AND NOTES

1. He, L.; Hannon, G. J. MicroRNAs: Small RNAs with a Big Role in Gene Regulation. *Nat. Rev. Genet.* **2004**, *5*, 522–531.
2. Calin, G. A.; Croce, C. M. MicroRNA Signatures in Human Cancers. *Nat. Rev. Cancer* **2006**, *6*, 857–866.
3. Filipowicz, W.; Bhattacharyya, S. N.; Sonenberg, N. Mechanisms of Post-transcriptional Regulation by MicroRNAs: Are the Answers in Sight? *Nat. Rev. Genet.* **2008**, *9*, 102–114.
4. Esquela-Kerscher, A.; Slack, F. J. Oncomirs - MicroRNAs with a Role in Cancer. *Nat. Rev. Cancer* **2006**, *6*, 259–269.
5. Esau, C. C.; Monia, B. P. Therapeutic Potential for MicroRNAs. *Adv. Drug Delivery Rev.* **2007**, *59*, 101–114.
6. He, L.; He, X.; Lim, L. P.; de Stanchina, E.; Xuan, Z.; Liang, Y.; Xue, W.; Zender, L.; Magnus, J.; Ridzon, D.; *et al.* A MicroRNA Component of the p53 Tumour Suppressor Network. *Nature* **2007**, *447*, 1130–1134.
7. Ma, L.; Teruya-Feldstein, J.; Weinberg, R. A. Tumour Invasion and Metastasis Initiated by MicroRNA-10b in Breast Cancer. *Nature* **2007**, *449*, 682–688.
8. Tavazoie, S. F.; Alarcon, C.; Oskarsson, T.; Padua, D.; Wang, Q.; Bos, P. D.; Gerald, W. L.; Massague, J. Endogenous Human MicroRNAs that Suppress Breast Cancer Metastasis. *Nature* **2008**, *451*, 147–152.
9. Medarova, Z.; Pham, W.; Farrar, C.; Petkova, V.; Moore, A. *In Vivo* Imaging of siRNA Delivery and Silencing in Tumors. *Nat. Med.* **2007**, *13*, 372–377.
10. Schetter, A. J.; Leung, S. Y.; Sohn, J. J.; Zanetti, K. A.; Bowman, E. D.; Yanaihara, N.; Yuen, S. T.; Chan, T. L.; Kwong, D. L. W.; Au, G. K. H.; *et al.* MicroRNA Expression Profiles Associated with Prognosis and Therapeutic Outcome in Colon Adenocarcinoma. *J. Am. Med. Assoc.* **2008**, *299*, 425–436.
11. Hwang, D. W.; Song, I. C.; Lee, D. S.; Kim, S. Smart Magnetic Fluorescent Nanoparticle Imaging Probes to Monitor MicroRNAs. *Small* **2010**, *6*, 81–88.
12. Whitehead, K. A.; Langer, R.; Anderson, D. G. Knocking Down Barriers: Advances in siRNA Delivery. *Nat. Rev. Drug Discovery* **2009**, *8*, 129–138.
13. Chen, Y.; Zhu, X.; Zhang, X.; Liu, B.; Huang, L. Nanoparticles Modified with Tumor-Targeting scFv Deliver siRNA and miRNA for Cancer Therapy. *Mol. Ther.* **2010**, *18*, 1650–1656.
14. Kim, E.; Jung, Y.; Choi, H.; Yang, J.; Suh, J.-S.; Huh, Y.-M.; Kim, K.; Haam, S. Prostate Cancer Cell Death Produced by the Co-delivery of Bcl-xL shRNA and Doxorubicin using an Aptamer-Conjugated Polyplex. *Biomaterials* **2010**, *31*, 4592–4599.
15. Liu, X.-Q.; Song, W.-J.; Sun, T.-M.; Zhang, P.-Z.; Wang, J. Targeted Delivery of Antisense Inhibitor of miRNA for Antiangiogenesis Therapy using cRGD-Functionalized Nanoparticles. *Mol. Pharm.* **2010**, *8*, 250–259.
16. Torchilin, V. P. Recent Advances with Liposomes as Pharmaceutical Carriers. *Nat. Rev. Drug Discov.* **2005**, *4*, 145–160.
17. Huang, Z.; King, M. R. An Immobilized Nanoparticle-Based Platform for Efficient Gene Knockdown of Targeted Cells in the Circulation. *Gene Ther.* **2009**, *16*, 1271–1282.

18. Harris, J. M.; Chess, R. B. Effect of Pegylation on Pharmaceuticals. *Nat. Rev. Drug Discov.* **2003**, *2*, 214–221.
19. Klibanov, A. L.; Maruyama, K.; Torchilin, V. P.; Huang, L. Amphipathic Polyethyleneglycols Effectively Prolong the Circulation Time of Liposomes. *FEBS Lett.* **1990**, *268*, 235–237.
20. Boussif, O.; Lezoualc'h, F.; Zanta, M. A.; Mergny, M. D.; Scherman, D.; Demeneix, B.; Behr, J. P. A Versatile Vector for Gene and Oligonucleotide Transfer into Cells in Culture and *in Vivo*: Polyethylenimine. *Proc. Natl. Acad. Sci. U.S.A.* **1995**, *92*, 7297–7301.
21. Luo, D.; Saltzman, W. M. Synthetic DNA Delivery Systems. *Nat. Biotechnol.* **2000**, *18*, 33–37.
22. Nitin, N.; Santangelo, P. J.; Kim, G.; Nie, S.; Bao, G. Peptide-Linked Molecular Beacons for Efficient Delivery and Rapid mRNA Detection in Living Cells. *Nucleic Acids Res.* **2004**, *32*, e58.
23. Turner, J. J.; Jones, S.; Fabani, M. M.; Ivanova, G.; Arzumanov, A. A.; Gait, M. J. RNA Targeting with Peptide Conjugates of Oligonucleotides, siRNA and PNA. *Blood Cells Mol. Dis.* **2007**, *38*, 1–7.
24. Aruffo, A.; Stamenkovic, I.; Melnick, M.; Underhill, C. B.; Seed, B. CD44 is the Principal Cell Surface Receptor for Hyaluronate. *Cell* **1990**, *61*, 1303–1313.
25. Bourguignon, L. Y. W.; Singleton, P. A.; Zhu, H.; Zhou, B. Hyaluronan Promotes Signaling Interaction Between CD44 and the Transforming Growth Factor β Receptor I in Metastatic Breast Tumor Cells. *J. Biol. Chem.* **2002**, *277*, 39703–39712.
26. Al-Hajj, M.; Wicha, M. S.; Benito-Hernandez, A.; Morrison, S. J.; Clarke, M. F. Prospective Identification of Tumorigenic Breast Cancer Cells. *Proc. Natl. Acad. Sci. U.S.A.* **2003**, *100*, 3983–3988.
27. Zhou, B.; Weigel, J.; Fauss, L.; Weigel, P. Identification of the Hyaluronan Receptor for Endocytosis (HARE). *J. Biol. Chem.* **2000**, *275*, 37733–37741.
28. Assmann, V.; Marshall, J.; Fieber, C.; Hofmann, M.; Hart, I. The Human Hyaluronan Receptor RHAMM Is Expressed as an Intracellular Protein in Breast Cancer Cells. *J. Cell Sci.* **1998**, *111*, 1685–1694.
29. McCourtl, P.; Eke, B.; Forsberg, N.; Gustafson, S. Intercellular Adhesion Molecule-1 is a Cell Surface Receptor for Hyaluronan. *J. Biol. Chem.* **1994**, *269*, 30081–30084.
30. Raver-Shapira, N.; Marciano, E.; Meiri, E.; Spector, Y.; Rosenfeld, N.; Moskovits, N.; Bentwich, Z.; Oren, M. Transcriptional Activation of miR-34a Contributes to p53-Mediated Apoptosis. *Mol. Cell* **2007**, *26*, 731–743.
31. Suzuki, H. I.; Yamagata, K.; Sugimoto, K.; Iwamoto, T.; Kato, S.; Miyazono, K. Modulation of MicroRNA Processing by p53. *Nature* **2009**, *460*, 529–533.
32. Liu, C.; Kelnar, K.; Liu, B.; Chen, X.; Calhoun-Davis, T.; Li, H.; Patrawala, L.; Yan, H.; Jeter, C.; Honorio, S.; *et al.* The MicroRNA miR-34a Inhibits Prostate Cancer Stem Cells and Metastasis by Directly Repressing CD44. *Nat. Med.* **2011**, *17*, 211–215.
33. Tyagi, S.; Kramer, F. R. Molecular Beacons: Probes that Fluoresce Upon Hybridization. *Nat. Biotechnol.* **1996**, *14*, 303–308.
34. Li, Q.; Luan, G.; Guo, Q.; Liang, J. A New Class of Homogeneous Nucleic Acid Probes Based on Specific Displacement Hybridization. *Nucleic Acids Res.* **2002**, *30*, e5.
35. Tsourkas, A.; Behlke, M. A.; Rose, S. D.; Bao, G. Hybridization Kinetics and Thermodynamics of Molecular Beacons. *Nucleic Acids Res.* **2003**, *31*, 1319–1330.
36. Huang, S.; Salituro, J.; Tang, N.; Luk, K.-C.; Hackett, J.; Swanson, P.; Cloherty, G.; Mak, W.-B.; Robinson, J.; Abravaya, K. Thermodynamically Modulated Partially Double-Stranded Linear DNA Probe Design for Homogeneous Real-Time PCR. *Nucleic Acids Res.* **2007**, *35*, e101.
37. Nayar, R.; Hope, M. J.; Cullis, P. R. Generation of Large Unilamellar Vesicles from Long-Chain Saturated Phosphatidylcholines by Extrusion Technique. *Biochim. Biophys. Acta-Biomembr* **1989**, *986*, 200–206.
38. Fujii, T.; Sun, Y.-L.; An, K.-N.; Luo, Z.-P. Mechanical Properties of Single Hyaluronan Molecules. *J. Biomech.* **2002**, *35*, 527–531.
39. Choi, K. Y.; Min, K. H.; Na, J. H.; Choi, K.; Kim, K.; Park, J. H.; Kwon, I. C.; Jeong, S. Y. Self-Assembled Hyaluronic Acid Nanoparticles as a Potential Drug Carrier for Cancer Therapy: Synthesis, Characterization, and *in Vivo* Biodistribution. *J. Mater. Chem.* **2009**, *19*, 4102–4107.
40. Oh, E. J.; Park, K.; Kim, K. S.; Kim, J.; Yang, J.-A.; Kong, J.-H.; Lee, M. Y.; Hoffman, A. S.; Hahn, S. K. Target Specific and Long-Acting Delivery of Protein, Peptide, and Nucleotide Therapeutics Using Hyaluronic Acid Derivatives. *J. Controlled Release* **2010**, *141*, 2–12.
41. Fattal, E.; Couvreur, P.; Dubernet, C. "Smart" Delivery of Antisense Oligonucleotides by Anionic pH-Sensitive Liposomes. *Adv. Drug Delivery Rev.* **2004**, *56*, 931–946.
42. Tokita, Y.; Okamoto, A. Hydrolytic Degradation of Hyaluronic Acid. *Polym. Degrad. Stab.* **1995**, *48*, 269–273.
43. Gura, E.; Hückel, M.; Müller, P. J. Specific Degradation of Hyaluronic Acid and Its Rheological Properties. *Polym. Degrad. Stab.* **1998**, *59*, 297–302.
44. Lee, Y.; Lee, H.; Kim, Y. B.; Kim, J.; Hyeon, T.; Park, H. W; Messersmith, P. B.; Park, T. G. Bioinspired Surface Immobilization of Hyaluronic Acid on Monodisperse Magnetite Nanocrystals for Targeted Cancer Imaging. *Adv. Mater.* **2008**, *20*, 4154–4157.
45. Wobus, M.; Rangwala, R.; Sheyn, I.; Hennigan, R.; Coila, B.; Lower, E. E.; Yassin, R. S.; Sherman, L. S. CD44 Associates with EGFR and ErbB2 in Metastasizing Mammary Carcinoma Cells. *Appl. Immunohistochem.* **2002**, *10*, 34–39.
46. Ghatak, S.; Misra, S.; Toole, B. P. Hyaluronan Constitutively Regulates ErbB2 Phosphorylation and Signaling Complex Formation in Carcinoma Cells. *J. Biol. Chem.* **2005**, *280*, 8876–8883.
47. Pályi-Krekk, Z.; Barok, M.; Kovács, T.; Saya, H.; Nagano, O.; Szöllosi, J.; Nagy, P. EGFR and ErbB2 are Functionally Coupled to CD44 and Regulate Shedding, Internalization and Motogenic Effect of CD44. *Cancer Lett.* **2008**, *263*, 231–242.
48. Carlsson, B.; Forsberg, O.; Bengtsson, M.; Tötterman, T. H.; Essand, M. Characterization of Human Prostate and Breast Cancer Cell Lines for Experimental T Cell-Based Immunotherapy. *Prostate* **2007**, *67*, 389–395.
49. Entwistle, J.; Hall, C. L.; Turley., E. A. HA Receptors: Regulators of Signaling to the Cytoskeleton. *J. Cell. Biochem.* **1996**, *61*, 569–577.
50. Wrobel, I.; Collins, D. Fusion of Cationic Liposomes with Mammalian Cells Occurs After Endocytosis. *Biochim. Biophys. Acta* **1995**, *1235*, 296–304.
51. Xu, Y.; Szoka, F. C. Mechanism of DNA Release from Cationic Liposome/DNA Complexes Used in Cell Transfection. *Biochemistry* **1996**, *35*, 5616–5623.
52. Mok, K. W.; Cullis, P. R. Structural and Fusogenic Properties of Cationic Liposomes in the Presence of Plasmid DNA. *Biophys. J.* **1997**, *73*, 2534–2545.
53. Vantyghem, S. A.; Wilson, S. M.; Postenka, C. O.; Al-Katib, W.; Tuck, A. B.; Chambers, A. F. Dietary Genistein Reduces Metastasis in a Postsurgical Orthotopic Breast Cancer Model. *Cancer Res.* **2005**, *65*, 3396–3403.